Fragmented Antenna Realization Using Coupled Small Radiating Elements

Navid Barani[ID], *Student Member, IEEE*, James F. Harvey, *Fellow, IEEE*, and Kamal Sarabandi, *Fellow, IEEE*

Abstract—This paper reports on the feasibility of formation of an electrically large antenna at low frequencies using a number of miniaturized antennas through electromagnetic coupling for achieving high bandwidth. The proposed fragmented antenna system is intended for a swarm of small unmanned aerial vehicles in a linear flight formation. Inductively end-loaded folded dipole antennas are used as radiating elements. The small antennas are designed so that they can individually radiate with small bandwidth when isolated. The overall dimensions and the total mass of these fabricated elements are $12 \times 10 \times 10$ cm ($0.096\lambda_0 \times 0.08\lambda_0 \times 0.08\lambda_0$ at 240 MHz) and 18 g (including the matching network), respectively. Each miniaturized antenna can only provide 2.4 MHz ($\sim$1%) bandwidth and 25 Ω input impedance. Having proper electromagnetic coupling between a cluster of three of such elements, measurement results demonstrate that the middle element can provide 18.4 MHz bandwidth (7.7%, 7.7 fold improvement) and 126 Ω input impedance when the other two elements are loaded with optimal reactive elements. Moreover, the proposed configuration shows 1 dB gain improvement at boresight direction. The effects of flight formation fluctuations on the coupled antennas are also investigated, and it is shown that as the separation distance between the coupled antennas increases, the input impedance and bandwidth enhancement decrease. To overcome this problem, a tunable matching circuit containing a single varactor is proposed. Measurement results are shown to be in good agreement with the simulation predictions.

Index Terms—Antenna miniaturization, bandwidth enhancement, coupled antenna array, unmanned aerial vehicle (UAV)-mounted antenna.

I. Introduction

ESTABLISHING reliable and short-range communication with low power in complex environments such as urban, indoor settings, and through caves is a challenging task. This is mainly because of the fact that in such complex environments, the presence of large number of scatterers, multipath, and shadowing leads to excessive signal attenuation and fast fading at microwave frequencies [1], [2]. These propagation phenomena severely affect the quality of the received signal and impose stringent conditions on the required

N. Barani and K. Sarabandi are with the Radiation Laboratory, Department of Electrical Engineering and Computer Science, University of Michigan, Ann Arbor, MI 48109-2122 USA (e-mail: nbarani@umich.edu; saraband@eecs.umich.edu).

J. F. Harvey is with the U.S. Army Research Office, Durham, NC 27703-9142 USA (e-mail: james.f.harvey.civ@mail.mil).

transmit power and signal processing [3]–[5]. In order to enhance the quality and reliability of a communication link in multipath-rich environments, different approaches such as cooperative routing with multiple radios and repeaters [6], [7], multiple-input and multiple-output systems [8], [9], or other diversity schemes [10] have been developed. In addition to the complexity and the cost, such systems typically require significant power which is a major concern for most *ad hoc* networks. To mitigate some of these adverse effects, operation at low frequencies (VHF and lower) is usually preferred especially for military applications [11]–[13]. The main reason is the fact that the wavelength is large or comparable to the size of most scatterers and thus, signals can penetrate significantly through the man-made and natural obstacles and produce far less reflection, scattering, and diffraction compared to what is observed at higher frequencies. Penetration through the soil and building materials at low frequencies allows for direct communication through multilayer walls and provides long distance coverage [14], [15]. Recent experimental studies are carried out to show communication between nodes inside and outside of buildings with many walls in between. Such studies prove that low-power and low-frequency radios can establish highly reliable communication links compare to, for example, a ZigBee radio operating at 2.4 GHz [3], [4].

Despite these advantages at low RF bands, the realization of compact systems is challenged by physically large antennas. This impediment makes the application of such systems limited to large vehicular or stationary nodes. In order to realize mobile communication systems, there is an essential need for extremely small antennas. Major drawbacks of miniaturized antennas are their narrow bandwidth and poor radiation efficiency. Of course, such narrow bandwidth limits the data rate significantly. Hence, the design of reasonably efficient, wideband, and miniaturized antennas is a critical task to enable compact, low-power, and low-frequency communication with high data rate. Although different types of miniaturization techniques providing better efficiency and bandwidth have been reported in [16]–[18], these are not sufficient for the application at hand. For small robotic platforms with relatively small form factors and constrained by their load capacity and available power, an alternative method must be considered for efficient radiation over wider bandwidth.

In recent years, several approaches have been introduced to design antennas for such platforms. Characteristic-mode theory is applied to design antennas for mobile metallic platforms [19], [20] basically by exploiting the metallic body as a large radiating aperture. However, this technique suf-
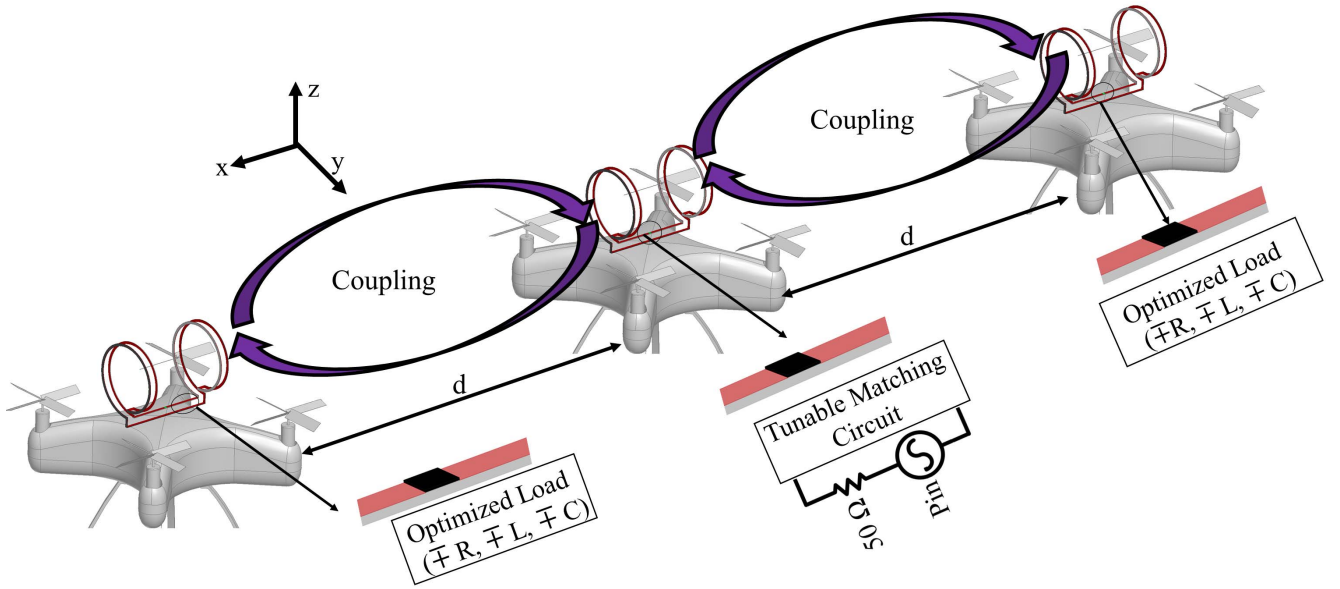
Fig. 1.   Proposed fragmented antenna concept for bandwidth enhancement of miniaturized antenna elements mounted on robotic flyers.

fers from really narrow bandwidth ($\leq 2.5\%$), unspecified polarization, and radiation pattern. Sarabandi *et al.* [21] and Sharawi *et al.* [22] utilize the wings of the robotic flyer to print and/or install antennas on them. The proposed printed dipole antenna in [21] has a relatively narrow bandwidth ($\leq \sim 4\%$) which may not be appropriate for certain applications requiring high data rate. Various types of planar antennas are also proposed for microwave bands [23], [24], intended to be directly attached to the body of the platform. Dimensions of these antennas are comparable to the wavelength, and they show wide impedance bandwidth ($\sim 20\%$). Such antennas are, of course, not compatible with the size of small robotic platforms at VHF bands. Thus, a new approach must be considered to design small antennas which can operate at VHF band and if needed can provide wider bandwidth with acceptable high radiation efficiency values. In this paper, the concept of near-field electromagnetic coupling (electric coupling + magnetic coupling) is applied to a cluster of three detached inductively end-loaded folded dipole antennas mounted on three separate mobile platforms in order to effectively realize a larger antenna and thus, provide wider bandwidth than that of a single element [25]. This concept is shown in Fig. 1. It is obvious that an antenna with large volume encompassing the cluster of coupled antennas provides a lower quality factor (Q) for the radiation and can effectively radiate electromagnetic waves over a wider bandwidth. For antenna excitation, different approaches have been used. In one approach, all the antennas are excited simultaneously. This method has the advantage of increasing the total radiated power; however, it is faced with the problem of source synchronization and lower efficiency which is due to the fact that the coupled powers will be dissipated in the other elements' source impedances. Another technique is to excite only the middle antenna, while the two adjacent antennas are loaded with lumped elements, as shown in Fig. 1. Application of several simple active and passive

load configurations (short circuit, open circuit, $\pm R$, $\pm L$, $\pm C$, and combination) is investigated, and an optimization approach is carried out to maximize a cost function that accounts for the improved fractional bandwidth and the average radiation efficiency ($\bar{\eta}$) over the band of operation. It is shown that the input impedance of the coupled antenna array is highly sensitive to its separation distance with each other requiring a tunable matching circuit. A tunable matching circuit is also proposed to overcome the problems associated with the flight formation fluctuations of the mobile platforms. The proposed fragmented antenna configuration, its design methodology, principle of operation, and the parametric studies are discussed in Section II. Fabrication and measurement results for return loss, radiation pattern, and peak gain are presented in Section III. Section IV finally provides the concluding remarks.

II. PROOF OF CONCEPT AND DESIGN APPROACH

A. Single-Antenna Design Considerations

Fig. 1 illustrates the proposed concept for bandwidth and radiation efficiency enhancement where a cluster of three equally separated miniaturized antennas implemented on three separate robotic flyers radiates and couples to each other electromagnetically in their near-field region. The components of the fragmented antenna are designed so that each piece can operate individually and be able to radiate signals albeit with lower bandwidth. The single radiating element, shown in Fig. 2, is an inductively end-loaded folded dipole antenna. For simulations and analysis, we have assumed that antennas are printed on Rogers RO4003C substrate ($\varepsilon_r = 3.55$ and $\tan \delta = 0.0027$). Wire antenna configuration is preferred for achieving low mass and ease of fabrication. There are also two reasons for using these end loads. The first reason, which will be discussed in detail in Section II-B, is that such inductive end loads can be used for near-field electromagnetic (electric+
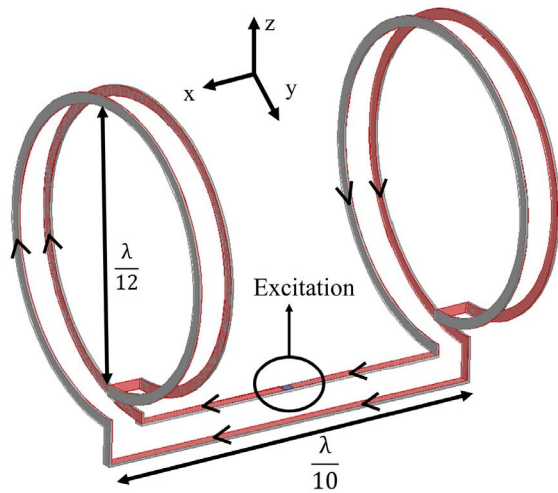
Fig. 2. Configuration of an inductively end-loaded folded dipole antenna element on a thin printed circuit board.

Fig. 4. Normal magnetic and electric field intensities (along the axis of end loads, *x*-axis) associated with the dipole, folded dipole, and threefold dipole antennas. (All the fields are normalized to the maximum field value which is for the threefold dipole antenna.)
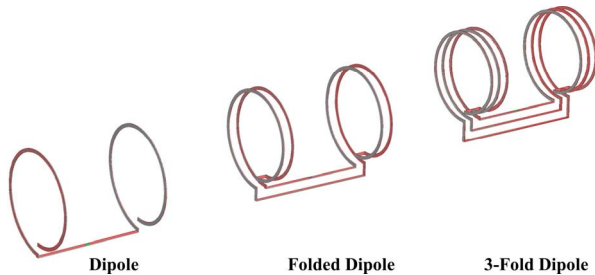

Fig. 3. Inductively end-loaded dipole antenna and its folded and threefold versions for coupling and input impedance enhancement.

magnetic) coupling between adjacent antennas and in effect, provide a large antenna electrical dimension for improved electromagnetic radiation over a wider bandwidth. It should be noted that by making the physical dimensions of the end loops larger, their near-field coupling range can be increased. The second reason is that the end loads are used to considerably reduce the linear dimension of the antennas [16], [17]. Using the inductive end loads, the length of the elements can be reduced to any desired level. In this paper, dimensions are reduced to have antennas to be confined within $12 \times 10 \times 10$ cm ($0.096\lambda_0 \times 0.08\lambda_0 \times 0.08\lambda_0$ at 240 MHz) to be able to implement each of them on very small mobile platforms as small as having maximum dimension of 15 cm. As mentioned earlier, miniaturizing antennas will lead to lower radiation resistance and make impedance matching more difficult. It is well known that folded dipole presents an input impedance four times that of the ordinary dipole. This is the reason that a folded structure is considered here. We also considered threefold and fourfold dipole structures that are appropriate for smaller size elements for fragmented antenna applications (see Fig. 3). It is expected that the impedance of smaller elements can be matched using threefold or fourfold elements. This is because of the fact that an *n*-fold dipole antenna has effectively n^2 times higher input impedance compared with that of the ordinary dipole antenna [26]. Full-wave simulations, carried out by HFSS software, show that the input impedance of the
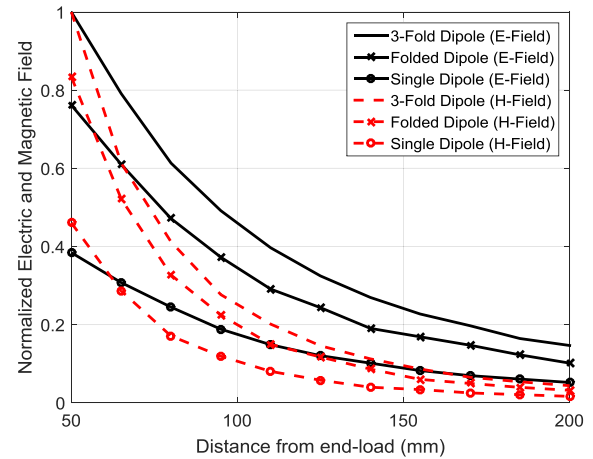
ordinary dipole antenna (with dimensions mentioned above) and its folded and threefold versions at the resonant frequency are 5.5, 25, and 55 Ω, respectively. Investigations are also carried out for coupling improvement. Such study is important because higher coupling between the separate antennas allows realization of the proposed fragmented antenna over longer distances for bandwidth enhancement. In addition to having inherently larger bandwidth, we expect that the *n*-fold dipole antenna can increase the extent of the near-field electromagnetic coupling. To prove this point, Fig. 4 illustrates the simulated electric- and magnetic-field intensities normal to the end loads along their axis for the three versions of the dipole antenna. The end-load diameter can also be increased to enhance the extent of the near-field range. But, in general, the optimal design is subject to the required miniaturization factor that determines the size and the number of the loops (number of folding for the dipole elements). Here, for the ease of fabrication and simple verification of the concept, we have just considered folded dipole antennas as the radiating elements. Another important factor is the direction of rotation of the end loops with respect to each other and that of their neighbor. Basically, for the two end loads of each antenna, it is important to figure out whether loops should be in the same direction. It was determined that if the directions are the same, the radiation associated with equivalent magnetic dipole of the end loops cancel out each other and does not affect the radiation associated with the dipole arms. This is important for achieving maximum polarization purity.

B. Coupling Mechanisms in Fragmented Coupled Antenna

Based on the proposed configuration for the fragmented coupled antenna, shown in Fig. 1, three coupling mechanisms between adjacent antennas can be identified, as depicted in Fig. 5. The first one is a magnetic (inductive) coupling between the end loops of the adjacent antennas via their normal magnetic fields (*x*-component). The second mechanism is an electric (capacitive) coupling between the dipole arms.
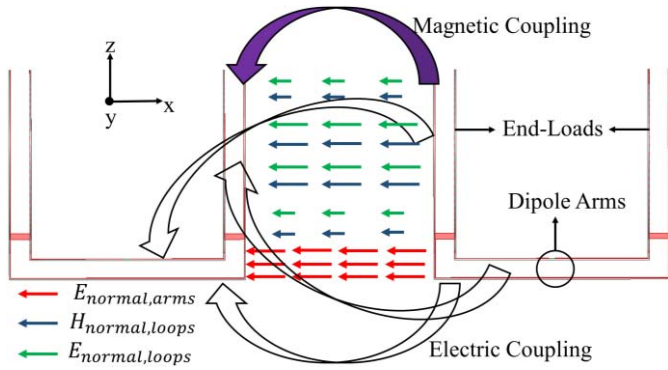
Fig. 5. Different coupling mechanisms between the adjacent antennas in the fragmented antenna configuration. (The end loops are in the *yz* plane, and the *x*-axis is along the axis of the loops.)
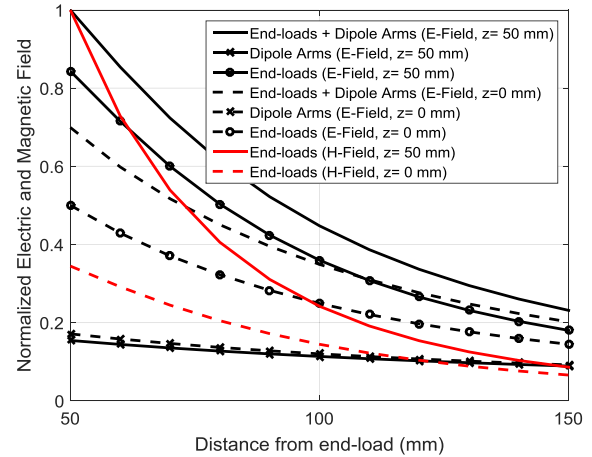

Fig. 6. Normal magnetic and electric field intensities (along the axis of end loads) associated with the dipole arms and end loads of a single-element antenna shown in Fig. 2.

As shown in Fig. 5, in the near-field region, the dipole arms of the inductively end-loaded folded dipole antenna have a very strong radial component that can couple to the dipole arms of the adjacent antennas efficiently. The third coupling mechanism is the capacitive coupling between the end loops and dipole arms. It is well known that loop antenna with nonuniform current distribution can have very strong electric field along its normal axis [27]. Thus, we expect that the inductive end loads, which resemble loop antenna with nonuniform current distribution, have strong normal electric field in their near-field region and thus, can couple to the dipole arms of the adjacent antennas efficiently. To quantify these couplings and investigate their effects accurately, CAD FEKO software (method of moment solver) is used for this section. In a software like FEKO, after performing full-wave simulation on a single inductively end-loaded folded dipole antenna, radiation from its different parts (end loads and dipole arms) can be analyzed separately. Fig. 6 illustrates the electric field and magnetic field profiles (normal to the end loads) of the two dipole arms and the four end loads associated with each of the single-element antennas as a function of distance from the end load (d). Observation lines are at $z = 0$ (along the dipole arms) and $z = 50$ mm (along the normal axis of the end loads) according to the given geometry for the single-element antenna (see Fig. 2). All the electric- and magnetic-field profiles are normalized to their corresponding maximum total field ($d = 50$ mm and $z = 50$ mm). As shown in Fig. 6, the electromagnetic radiation in the near-field region is basically dominant by the end loads rather than the dipole arms. This is because of the fact that the dipole arms are electrically small ($\lambda/10$), whereas the end loops have the total length of approximately $4\lambda/10$. Next, the magnetic field profile associated with the end loops decays faster compared to electric field profile and consequently, magnetic coupling is more sensitive to the distance between the adjacent antennas. It should be noted that the dipole arms have no normal magnetic field (x-component). That is why only the normal magnetic field associated with the end loads is plotted in Fig. 6. Another important point is that in our region of interest (100–150 mm), the electric coupling between the end loads and dipole arms is stronger than the electric coupling between

the dipole arms. In summary, the antennas in the proposed configuration are coupled to each other electromagnetically (combination of both electric and magnetic coupling).

C. Fragmented Antenna Design Methodology

So far, we have considered the single-antenna design challenges and investigated the coupling mechanisms between the antennas. Now, the design approach of the proposed antenna geometry for bandwidth enhancement is explained. In this paper, we only consider excitation of the middle antenna as the driver while the two adjacent antennas are to be terminated with appropriate lumped-element loads, as shown in Fig. 1. When the current flows on the excited antenna's arms, this antenna not only radiates into the free space, but also couples to the adjacent antennas. The coupled signal will be received and reflected back by the terminals of the adjacent elements and results in a current flow on their arms. Therefore, these elements assist the excited antenna to better radiate into the free space. Hereafter, we refer to the two adjacent antennas as "assistive antennas" and the middle antenna as "driver antenna." It is apparent that the larger the reflection coefficient of the loads, the higher can be the radiation efficiency if all radiations are in-phase. However, this condition may not necessarily provide a reasonable return loss for the driver antenna noting that the assistive antennas are coupling back to the driver antenna. For this reason, variations of several loads including short circuit, open circuit, purely resistive loads, inductive loads, capacitive loads, and combination of the passive and active loads are considered to examine whether efficient radiation over wider bandwidth can be achieved. It is expected that the application of resistive loads will result in considerable bandwidth enhancement, but this enhancement is mainly due to the dissipation of coupled power in the resistive loads. In this case, the radiation efficiency becomes really poor. On the other hand, the application of purely reactive loads (capacitive or inductive) will not adversely affect the radiation efficiency but can still improve the bandwidth due to the radiation resistance of the assistive elements. It should

be noted that the reactive loads can reflect a portion of the power which is partially radiated and partially coupled back to the driver antenna port which in turn adversely affect the return loss. Thus, for any arbitrary load configuration, there is a tradeoff between bandwidth enhancement and the radiation efficiency. An optimization must be carried out for various load configurations to maximize a cost function defined as

$$C(\text{load}) = \alpha \frac{\Delta f}{f_0} + \beta \bar{\eta}. \qquad (1)$$

Here, α and β are two constants normalizing the influence of the fractional bandwidth and the average (over the operating band) efficiency. The proposed cost function accounts for both bandwidth enhancement and average radiation efficiency over the -10 dB S_{11} bandwidth. The two constants can be chosen to emphasize the bandwidth or the average radiation efficiency or give them equal weight. Noting that the radiation efficiency can attain a maximum value of 100% and the desired fractional bandwidth is 10%, we set $\alpha = 10$ and $\beta = 1$ to give equal weight to average efficiency and the fractional bandwidth. In the analysis that follows, it is assumed that both assistive antennas are terminated with identical loads to ensure symmetry in the radiation pattern of the combined antenna configuration. The optimized load is calculated initially assuming that the separation distance (d) between the adjacent antennas is fixed and equal to one single element's length which is 12 cm. Full-wave simulations are carried out for various aforementioned load configurations to maximize $C(\text{load})$. The simulation results demonstrate that for $d = 12$ cm, the optimized load is a purely capacitive load with a capacitance value of $C = 4.4$ pF. Fig. 7(a) and (b) shows the comparison of the fragmented antenna reflection coefficient (S_{11}) and radiation efficiency over its S_{11} bandwidth using the optimized capacitive load with the antenna configuration with a purely resistive load ($R = 36\ \Omega$), a purely inductive load ($L = 15$ nH), and also with that of the single radiating element. Full-wave simulations illustrate that the proposed single-element miniaturized antenna provides 25 Ω input impedance and bandwidth of 2.4 MHz (1%). As can be concluded from Fig. 7(a) and (b), the application of resistive load shows considerable bandwidth enhancement; however, its radiation efficiency, as expected, is very low. Moreover, based on these simulation results, loading the assistive antennas with the optimized capacitive load results in 16 MHz (6.7%) bandwidth while the optimized inductive load provides 14.5 MHz (6.04%) bandwidth. Loading the assistive antennas with capacitors actually shifts the center frequency to the higher frequencies (>240 MHz), whereas for the inductive loads, this shift is toward lower frequencies (<240 MHz). As a result, the overall electrical length of the fragmented coupled antenna with capacitve loads is larger than that of the inductive loads. Hence, more bandwidth is expected to be achieved for the capacitive load. In Fig. 7(b), It is shown that the average radiation efficiency using reactive loads is 97% over the respective S_{11} bandwidths. It is also interesting to note that the fragmented antenna configuration shows one additional resonance due to the electromagnetic coupling of the assistive antennas with
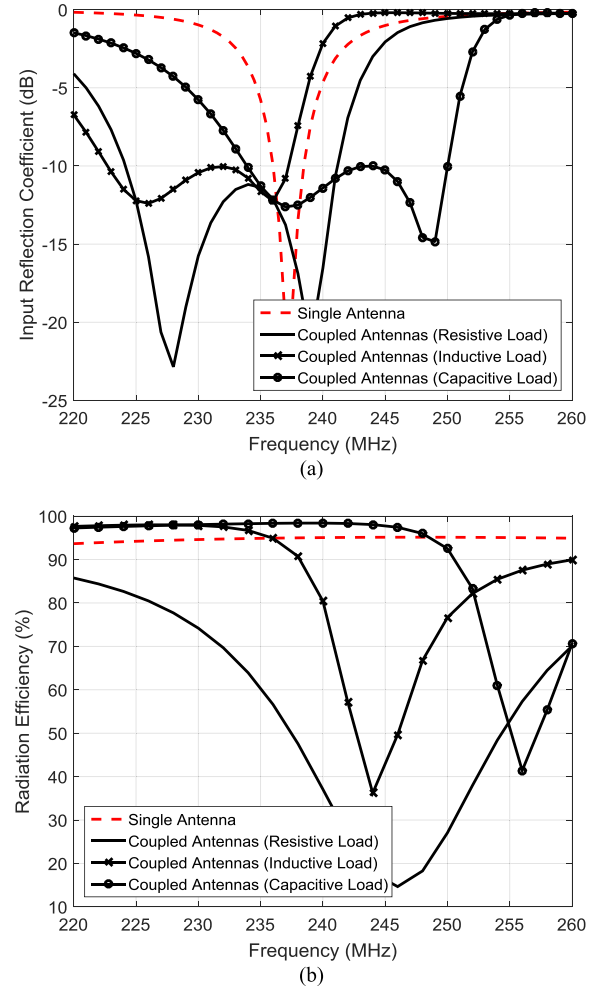

Fig. 7. Performance analysis of the coupled antennas with optimized load and other possible load configurations in terms of (a) bandwidth and (b) radiation efficiency. (The radiation efficiency is important only over the -10 dB return loss bandwidth.)

the driver antenna. This phenomenon can be explained as follows. The resonant frequency of the assistive antennas will shift due to the capacitive loading. Since these antennas couple to each other, the fragmented coupled antenna should include both the original resonance of the driver antenna and the new resonance of the assistive antennas. In fact, the enhanced bandwidth of the proposed approach is basically the result of combining different resonances together via the electromagnetic coupling between the inductive end loads and dipole arms. Fig. 8 illustrates this phenomenon clearly for the capacitive load ($C = 4.4$ pF), in which the achieved bandwidth is shown to contain the resonant frequency of the driver antenna and the resonant frequency of the assistive antennas loaded with the optimized series capacitor.

D. Sensitivity Analysis

As mentioned earlier, individual antennas are intended to be placed on very small mobile platforms such as robotic flyers. These platforms typically have small form factor and are highly prone to fluctuations during the flights. For example, the separation distance (d) between the platforms may fluctuate during the flight. In addition, the antennas on
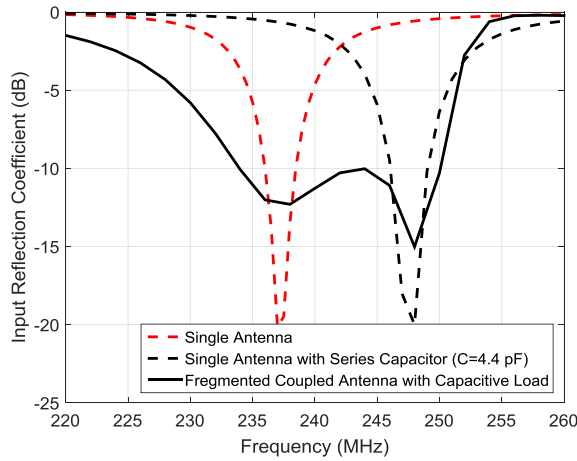
Fig. 8.   Formation of double resonances in the fragmented antenna configuration.
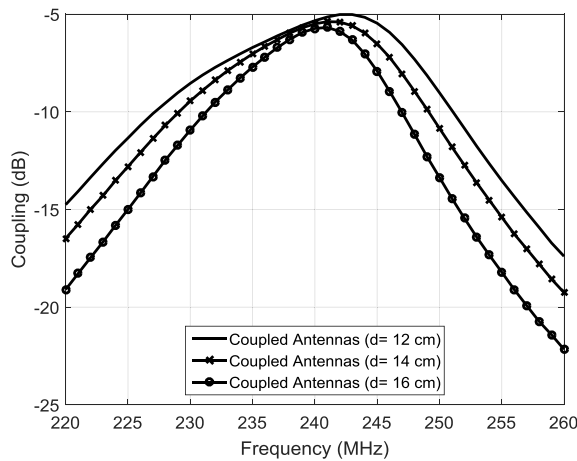

(a)

Fig. 9.   Coupling (S_{21} or S_{31}) between the driver antenna and each of the two assistive antennas.
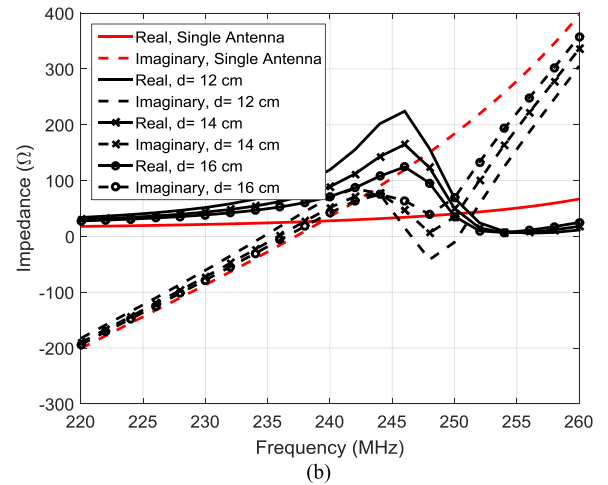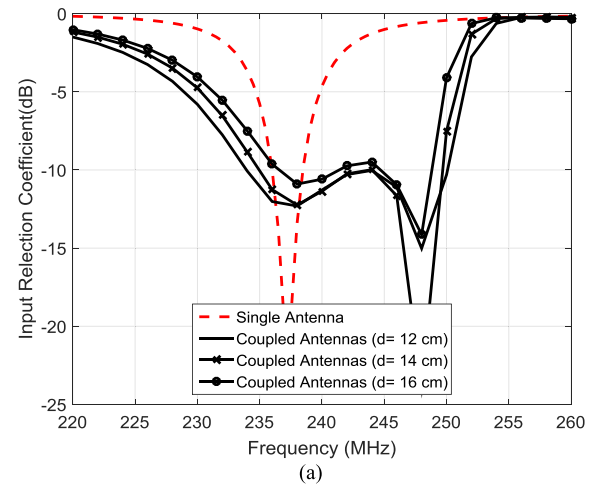

(b)

Fig. 10.   (a) Separation distance effect on the bandwidth of the proposed coupled array configuration. (b) Variation of the real and the imaginary parts of the input impedance for different separation distances.
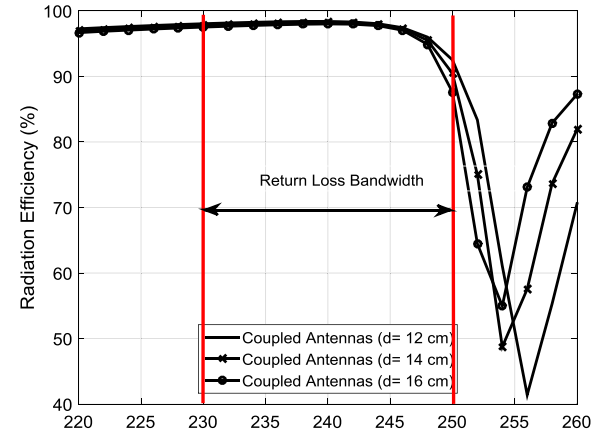

Fig. 11.   Simulated radiation efficiency for different separation distances.

the platforms may not be exactly aligned to achieve maximum coupling. To examine such uncertainties, full-wave simulations are carried out to determine bandwidth degradation as a result of such fluctuations. The separation distance (d) between the antennas is varied between 12 and 16 cm while maintaining the alignment of the axes of the end loops. Fig. 9 illustrates the coupled signal (S_{21} or S_{31}) from the middle (driver) antenna to each of the two assistive antennas. As expected, the longer the separation distance, the lower is the antennas mutual coupling. This is primarily due to the fact that electromagnetic fields generated by the inductive end loads decay rapidly away from the center [26], as shown in Fig. 4. The return loss and input impedance associated with the fragmented antenna configuration for three separation distances are obtained through full-wave simulations and shown in Fig. 10(a) and (b), respectively. As the separation distance between the elements increases, the input impedance and bandwidth enhancement decrease gradually mainly because of the weaker electromagnetic coupling between the antennas. Fig. 11 also depicts the simulated radiation efficiency for the mentioned separation distances. It is apparent that the radiation efficiency is not sensitive to the distance between the antennas. The calculated average radiation efficiency over the input return loss bandwidth is

approximately 97% for all the separation distances (d) and higher than that for the single antenna (95%). The simulation for the radiation efficiency does not consider the effect of Q-factor associated with the capacitive loads because capacitors typically have very large values for their Q (100–1000) at low frequencies (VHF band). Table I reports the input impedance (Z_{in}) of the antenna configuration. In all return loss and radiation efficiency simulations, it is assumed that

Antenna Configuration	$Z_{in}(\Omega)$	BW (MHz)	$\bar{\eta}$ (%)
Single Antenna	25	2.4	95
Coupled Antennas (d= 12cm)	126	16	97
Coupled Antennas (d= 14cm)	110	15	97
Coupled Antennas (d= 16cm)	100	13.5	97

Fig. 13. Single inductively end-loaded folded dipole antenna mounted on a small dielectric-made ($\varepsilon_r = 4$) quadcopter. (a) 3-D view. (b) Top view.

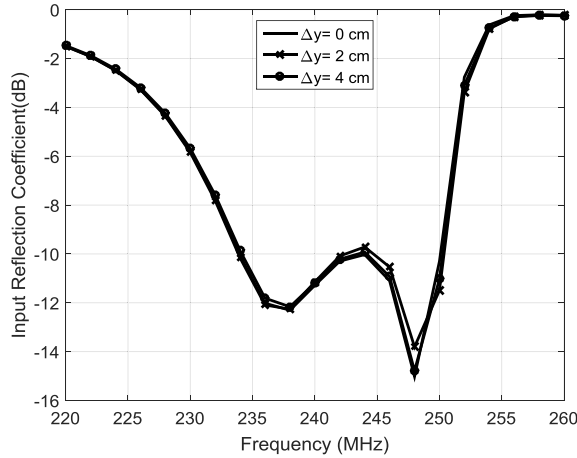Fig. 12. Effect of misalignment of the inductive end loads along the y-direction on the bandwidth of the proposed antenna configuration.

Fig. 14. Simulation results for comparison between the performance of coupled antennas in the presence and absence of the platform.

the source impedance connected to the driver antenna is equal to Z_{in}. Next, the sensitivity of the coupled antenna bandwidth to misalignment in horizontal plane (the y-axis) is examined. The two assistive antennas are located at a fixed separation distance ($d = 12$ cm) from the driven antenna, and both of them are shifted along the y-axis by Δy cm (see Fig. 1). Fig. 12 illustrates the simulated reflection coefficient for this configuration for two displacement values. It is obvious that the fragmented coupled antennas' bandwidth is not highly sensitive to misalignment of the assistive antennas in lateral directions. Not much bandwidth degradation is observed for lateral displacement as high as the end-loop radius. The reason for such observation is that the dipole arms and end loops have relatively wide electromagnetic field profiles in their near-field region in the yz plane which maintain the coupling constant. In practice, unmanned aerial vehicles (UAVs) are typically equipped with IR range sensors that give them an ability to have accurate estimation of their position relative to other UAVs during the flight in order to maintain a desired flight formation.

E. Platform Effects on Fragmented Antenna's Performance

Another challenge associated with the placement of the fragmented antenna on the mobile platforms is the presence of the platform itself as a scatterer around the antenna system. Small UAV structures are usually made with composite materials (nonmetallic). This is mainly due to the fact that composite materials are much lighter and low cost, and are much easier to fabricate. It is then expected that the presence of platform itself would not significantly affect the performance of the
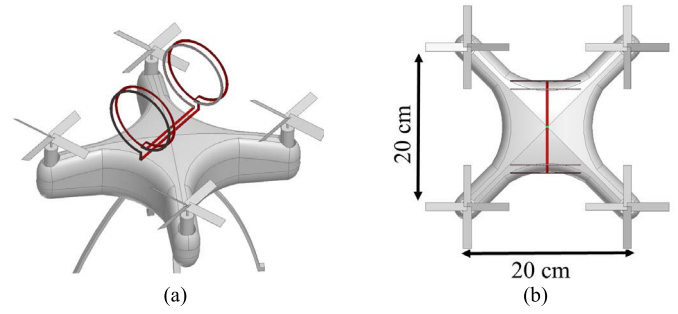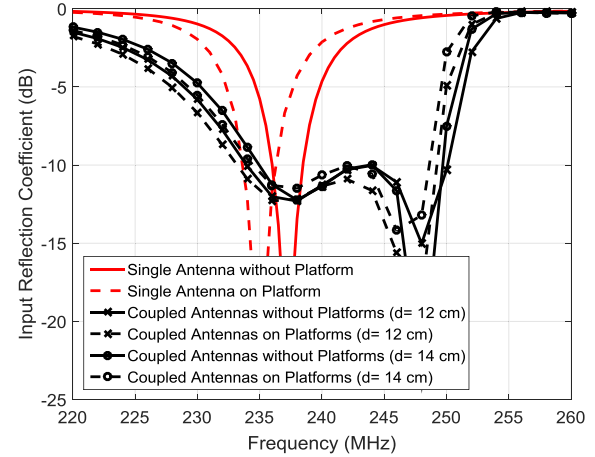
antenna system. To demonstrate this, an individual inductively end-loaded folded dipole antenna is placed over a dielectric UAV model, as shown in Fig. 13. A composite material with a dielectric constant of $\varepsilon_r = 4$ is chosen for the body of the UAV. The same full-wave simulations with the same values for the capacitance and port's input impedances as in Section II-D are carried out in this investigation. Fig. 14 illustrates the results for these simulations. It is shown that the presence of the dielectric platform can only cause a very small shift in the center frequency of the operating band which can be accounted for at the design stage. This is because of the fact that the platforms are still much smaller than the operating wavelength ($\sim\lambda/6$) and occupy a small fractional volume around the antenna. Therefore, their perturbation effects on the radiating electromagnetic field are negligible. Finally, it should be emphasized that if the antennas are intended for metallic platforms, the platform and antenna should be co-designed to account for platform–antenna interactions.

F. Tunable Matching Circuit

As observed in Section II-D, deviation from desired flight formation can change the input impedance of the driver antenna. Also, it was mentioned that the antenna on the UAV is expected to operate individually (single element) in the absence of the assistive elements. As indicated in Table I, the range of the input impedance varies from 25 Ω for the isolated antenna to 126 Ω for perfectly coupled antennas at a set minimum distance $d = 12$ cm. On the other hand, common
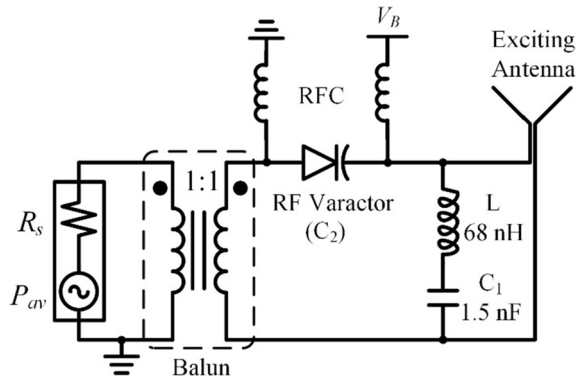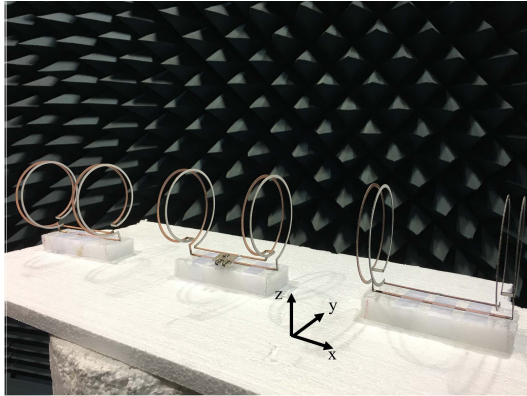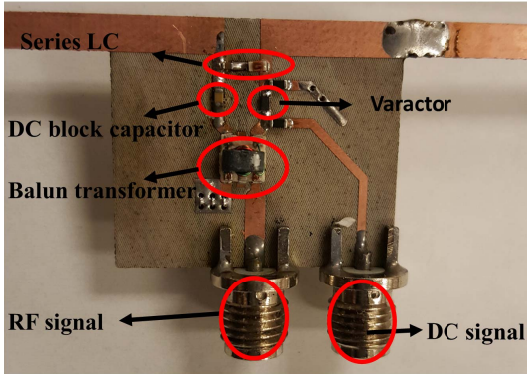
Fig. 15. Proposed tunable matching circuit containing a tuning diode (varactor).

(a)

(b)

Fig. 16. (a) Fabricated antennas inside anechoic chamber. (b) Fabricated tunable matching circuit integrated with the driver antenna.

radios operate with source impedance of 50 Ω. This requires a tunable matching circuit to ensure maximum power transfer to the antenna configuration for all possible cases. A simple tunable matching network is proposed based on an L-section LC circuit [28] consisting of one fixed capacitor ($C_1 = 1.5$ nF), one fixed inductor ($L = 68$ nH), one variable capacitor varactor (controlled by a dc voltage V_B), and one Balun transformer, as shown in Fig. 15. Two large inductors ($L_{RFC} = 3.3 \ \mu$H) are also used as RF chokes in the biasing network of the varactor. The required capacitor (C_2) for $d = 12$, 14, and 16 cm is calculated to be 6.8, 8.8, and 8.94 pF, respectively. Based on the required range of the variable capacitor (C_2), a varactor diode from the Infineon Technology,
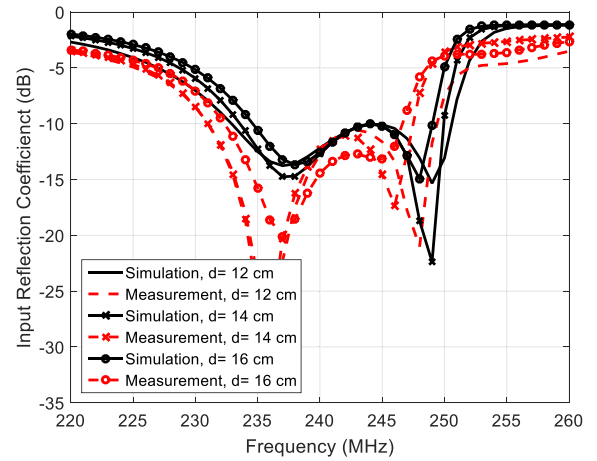

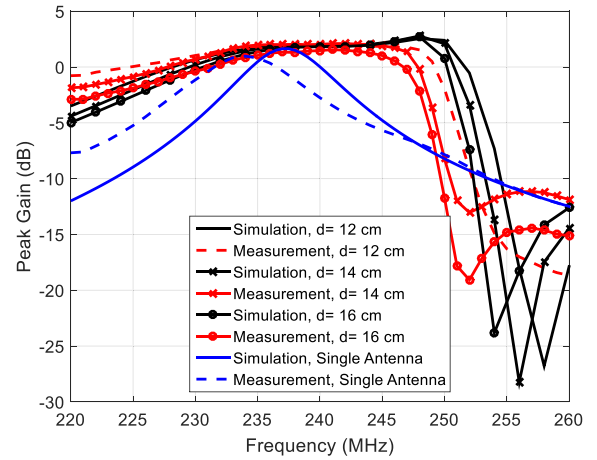Fig. 17. Measured and simulated return loss for the different separation distances.

Fig. 18. Measured and simulated peak gain (in the boresight direction) over band for the different separation distances.

Neubiberg, Germany, (BBY53-02L) is chosen. According to the C–V curve of this varactor diode, the required reverse voltage (V_B) at each separation distance is 2.06, 1.88, and 1.86 V, respectively. It should be noted that all the simulations associated with the matching circuit are performed using ADS. This circuit is fabricated and integrated with driver antenna. The simulation results are compared with the measurement results and reported in Section III.

III. FABRICATION AND MEASUREMENT RESULTS

The array of three coupled inductively end-loaded folded dipole antennas described in Section II is fabricated for measurement and comparison with the simulation results. The fabricated antennas and the tunable matching circuit are illustrated in Fig. 16(a) and (b), respectively. The dipole arms and inductive end loads are fabricated separately and then soldered together to construct a 3-D antenna geometry. All the components are fabricated with low-cost substrate (RO4003C). In practice, however, the antennas are to be fabricated with thin copper-coated steel wires to make sure that they are structurally stable. As can be seen from Fig. 16(a), the assistive antennas' end loops are wounded in the opposite direction of the corresponding end loops of the driver antenna.
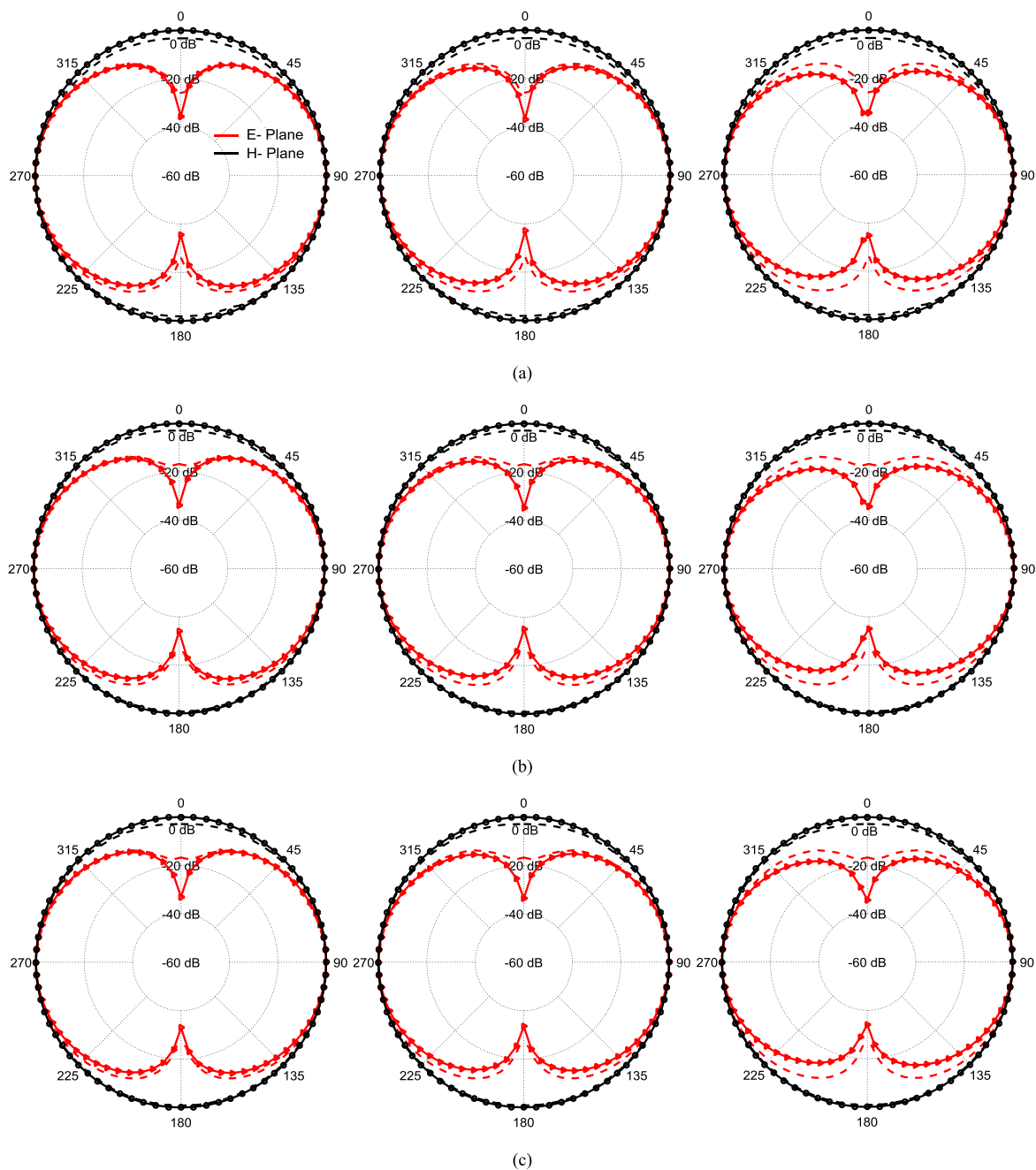
Fig. 19. Measured and simulated radiation pattern in E-plane (red) and H-plane (black) for three different frequencies (from left to right: 234, 240, and 246 MHz) over the achieved frequency bandwidth. (a) $d = 12$. (b) $d = 14$. (c) $d = 16$ cm. The solid lines are simulations, and the dashed lines are measurements.

TABLE II
IMPEDANCE BANDWIDTH AND PEAK-GAIN VARIATION IN THE IMPEDANCE BANDWIDTH (SIMULATION AND MEASUREMENT)

Antenna Configuration	Simulated -10 dB Impedance Bandwidth	Simulated Peak-Gain Variation in Impedance Bandwidth	Measured -10 dB Impedance Bandwidth	Measured Peak-Gain Variation in Impedance Bandwidth
Single Antenna	236 MHz- 238.4 MHz	1.26 dB -1.64 dB	232.9 MHz- 235.3 MHz	0.56 dB- 0.97 dB
Coupled antennas (d=12 cm)	232.9 MHz- 250.7 MHz	1.36 dB- 2.54 dB	231 MHz- 249.4 MHz	0.1 dB- 1.94 dB
Coupled antennas (d=14 cm)	233.6 MHz- 249.9 MHz	1.34 dB- 2.78 dB	231 MHz- 247.4 MHz	0.8 dB- 2.1 dB
Coupled antennas (d=16 cm)	234.9 MHz- 249 MHz	1.34 dB- 2.69 dB	232.4 MHz- 246.8 MHz	0.2 dB- 1.6 dB

This way, the magnetic field associated with the adjacent loops of all three antennas will amplify each other and results in a stronger coupling. Fig. 17 depicts both the measured and simulated reflection coefficient (S_{11}) of the proposed coupled antenna array for the aforementioned separation distances. It should be noted that in the simulation results,

the effect of the matching circuit has been considered. The measured -10 dB return loss bandwidth is given in Table II. It is shown that for $d = 12$ cm, the fragmented coupled antenna can provide 18.4 MHz bandwidth (7.7%) which is 7.7 times improvement over the isolated antenna bandwidth. In addition, as the separation distance (d) increases, the bandwidth enhancement decreases. A very good agreement between simulation and measurement results can also be seen. For the radiation pattern and peak-gain measurements, one wideband log-periodic dipole array antenna operating from 200 MHz to 2 GHz (model 3148B) is used. A calibrated vector network analyzer is used to measure the S_{21} between the log-periodic antenna and the proposed coupled antennas inside the anechoic chamber of the University of Michigan, Ann Arbor, MI, USA. Fig. 18 illustrates the measured and simulated peak gain (boresight direction) over the entire bandwidth. It should be noted that the discrepancy between the simulations and measurements for the peak gain is mainly due to the loss associated with the Balun transformer. Based on its data sheet, the Balun transformer has approximately 0.7 dB of insertion loss. As expected, the peak-gain variation is not highly sensitive to the separation distance between the antennas. Figs. 17 and 18 show a very small frequency shift in the measurement results compared with that of the simulation results. This is mainly because of the imperfections in the fabrication process and also the tolerance of the lumped-element loads used in the assistive antennas and matching network of the driver antenna. The information regarding variation of the peak gain over the S_{11} bandwidth associated with each separation distance is given in Table II. It is important to mention that the proposed fragmented coupled antenna not only enhances the bandwidth but also provides a higher peak gain (around 1 dB) compared to the single-element antenna. The measured radiation efficiencies for $d = 12, 14,$ and 16 cm are also found to be 86.4%, 88.2%, and 80.4%, respectively. These smaller values for the measured radiation efficiencies compared with the simulated ones (97%) can be attributed to the insertion loss of the Balun transformer. Finally, the radiation patterns in the E-plane (xy plane) and the H-plane (yz plane) are measured for all the separation distances at the beginning, middle, and the end of the achieved frequency band (234, 240, and 246 MHz), as shown in Fig. 19. The radiation patterns resemble that of a dipole antenna with higher directivity.

IV. Conclusion

In this paper, the concept of fragmented coupled antenna for achieving high-bandwidth and high-gain radiating structure from an ensemble of very small elements on small moving platforms is presented. To enable isolated platform operating, a miniaturized folded dipole antenna with inductive end loads is designed. The provision of the inductive end loads is to enable electromagnetic coupling of three or more of such antennas carried out by separate flyers. To achieve high radiation efficiency, the middle antenna (driver antenna) is excited and the two adjacent antennas (assistive antennas) are terminated with lumped-element load. An optimization is carried on the load configuration to achieve considerable

bandwidth enhancement and high radiation efficiency. Measurement results demonstrate that for a separation distance between three of such antennas, equal to the length of each antenna (12 cm), the proposed configuration provides 7.7 times larger bandwidth (7.7%) than the bandwidth of the isolated antenna and results in an average radiation efficiency of above 86.4%. The coupled triple antenna configuration also shows 1 dB improvement in the peak gain compared with that of the single-element antenna. As the separation distance between the antennas increases, the bandwidth enhancement decreases. Effect of flight instabilities on the coupled array antennas is also investigated, and a tunable matching circuit using varactor diode is proposed so that the source can deliver maximum power to the antenna in all conditions.

References

[1] Y. Corre and Y. Lostanlen, "Three-dimensional urban EM wave propagation model for radio network planning and optimization over large areas," *IEEE Trans. Veh. Technol.*, vol. 58, no. 7, pp. 3112–3123, Sep. 2009.
[2] E. F. T. Martijn and M. H. A. J. Herben, "Characterization of radio wave propagation into buildings at 1800 MHz," *IEEE Antennas Wireless Propag. Lett.*, vol. 2, no. 1, pp. 122–125, Feb. 2005.
[3] F. T. Dagefu, J. Choi, M. Sheikhsofla, B. M. Sadler, and K. Sarabandi, "Performance assessment of lower VHF band for short-range communication and geolocation applications," *Radio Sci.*, vol. 50, pp. 443–452, May 2015.
[4] F. T. Dagefu *et al.*, "Short-range low-VHF channel characterization in cluttered environments," *IEEE Trans. Antennas Propag.*, vol. 63, no. 6, pp. 2719–2727, Jun. 2015.
[5] J. Andrusenko, R. L. Miller, J. A. Abrahamson, N. M. M. Emanuelli, R. S. Pattay, and R. M. Shuford, "VHF general urban path loss model for short range ground-to-ground communications," *IEEE Trans. Antennas Propag.*, vol. 56, no. 10, pp. 3302–3310, Oct. 2008.
[6] Y. J. Song and K. Sarabandi, "A simultaneous dual-channel micro-radio-repeater for ad-hoc wireless communication," *IEEE Trans. Antennas Propag.*, vol. 62, no. 6, pp. 3378–3383, Jun. 2014.
[7] Y. J. Song and K. Sarabandi, "Miniaturized radio repeater for enhanced wireless connectivity of ad-hoc networks," *IEEE Trans. Antennas Propag.*, vol. 60, no. 8, pp. 3913–3920, Aug. 2012.
[8] S. Alamouti, "A simple transmit diversity technique for wireless communications," *IEEE J. Sel. Areas Commun.*, vol. 16, no. 8, pp. 1451–1458, Oct. 1998.
[9] D. Gesbert, M. Shafi, D. Shiu, P. J. Smith, and A. Naguib, "From theory to practice: An overview of MIMO space-time coded wireless systems," *IEEE J. Sel. Areas Commun.*, vol. 21, no. 3, pp. 281–302, Apr. 2003.
[10] D. Tse and P. Viswanath, *Fundamentals of Wireless Communication*. Cambridge, U.K.: Cambridge Univ. Press, 2005.
[11] D. G. Lopez, M. Ignatenko, and D. S. Filipovic, "Low-profile tri-band inverted-F antenna for vehicular applications in HF and VHF bands," *IEEE Trans. Antennas Propag.*, vol. 63, no. 11, pp. 4632–4639, Nov. 2015.
[12] T.-Y. Shih and N. Behdad, "Bandwidth enhancement of platform-mounted HF antennas using the characteristic mode theory," *IEEE Trans. Antennas Propag.*, vol. 64, no. 7, pp. 2648–2659, Jul. 2016.
[13] M. Kashanianfard and K. Sarabandi, "Vehicular optically transparent UHF antenna for terrestrial communication," *IEEE Trans. Antennas Propag.*, vol. 65, no. 8, pp. 3942–3949, Aug. 2017.
[14] R. A. Dalke, C. L. Holloway, P. McKenna, M. Johansson, and A. S. Ali, "Effects of reinforced concrete structures on RF communications," *IEEE Trans. Electromagn. Compat.*, vol. 42, no. 4, pp. 486–496, Nov. 2000.
[15] S. Y. Lim, Q. P. Soo, A. Adam, D. W. G. Lim, Z. Yun, and M. F. Iskander, "Towards a comprehensive ray-tracing modeling of an urban city with open-trench drains for mobile communications," *IEEE Access*, vol. 5, pp. 2300–2307, 2017.
[16] R. Azadegan and K. Sarabandi, "A novel approach for miniaturization of slot antennas," *IEEE Trans. Antennas Propag.*, vol. 51, no. 3, pp. 421–429, Mar. 2003.
[17] N. Behdad and K. Sarabandi, "Bandwidth enhancement and further size reduction of a class of miniaturized slot antennas," *IEEE Trans. Antennas Propag.*, vol. 52, no. 8, pp. 1928–1935, Aug. 2004.

[18] H. Mosallaei and K. Sarabandi, "Antenna miniaturization and bandwidth enhancement using a reactive impedance substrate," *IEEE Trans. Antennas Propag.*, vol. 52, no. 9, pp. 2403–2414, Sep. 2004.

[19] Y. Chen and C.-F. Wang, "Electrically small UAV antenna design using characteristic modes," *IEEE Trans. Antennas Propag.*, vol. 62, no. 2, pp. 535–545, Feb. 2014.

[20] N. Barani, B. Yektakhah, and K. Sarabandi, "Parasitic antennas for small metallic platforms," in *Proc. IEEE Int. Symp. Antennas Propag. USNC/URSI Nat. Radio Sci. Meeting*, Jul. 2017, pp. 1995–1996.

[21] K. Sarabandi, J. Oh, L. Pierce, K. Shivakumar, and S. Lingaiah, "Lightweight, conformal antennas for robotic flapping flyers," *IEEE Antennas Propag. Mag.*, vol. 56, no. 6, pp. 29–40, Dec. 2014.

[22] M. S. Sharawi, D. N. Aloi, and O. A. Rawashdeh, "Design and implementation of embedded printed antenna arrays in small UAV wing structures," *IEEE Trans. Antennas Propag.*, vol. 58, no. 8, pp. 2531–2538, Aug. 2010.

[23] X. Zhao, S. P. Yeo, and L. C. Ong, "Planar UWB MIMO antenna with pattern diversity and isolation improvement for mobile platform based on the theory of characteristic modes," *IEEE Trans. Antennas Propag.*, vol. 66, no. 1, pp. 420–425, Jan. 2018.

[24] X. Zhao, B. N. Tian, S. P. Yeo, and L. C. Ong, "Wideband segmented loop antenna with dual-polarized omnidirectional patterns for mobile platforms," *IEEE Trans. Antennas Propag.*, vol. 56, no. 2, pp. 883–886, Feb. 2017.

[25] N. Barani and K. Sarabandi, "Antenna bandwidth enhancement using near-field coupled miniaturized elements," in *Proc. IEEE Int. Symp. Antennas Propag. (APSURSI)*, Jun./Jul. 2016, pp. 1727–1728.

[26] C. A. Balanis, *Antenna Theory: Analysis and Design*, 3rd ed. Hoboken, NJ, USA: Wiley, 2005.

[27] G. Glinski, "Note on circular loop antennas with non-uniform current distribution," *J. Appl. Phys.*, vol. 18, no. 7, pp. 638–644, 1947.

[28] D. M. Pozar, *Microwave Engineering*, 3rd ed. Hoboken, NJ, USA: Wiley, 1990.
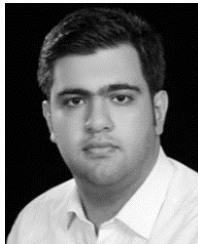
Navid Barani (S'16) was born in Isfahan, Iran in 1991. He received the B.S. degree in electrical engineering along with another B.S. degree in physics from the Isfahan University of Technology, Isfahan, Iran, in 2015. He is currently pursuing the Ph.D. degree in applied electromagnetics and RF circuits with the University of Michigan, Ann Arbor, MI, USA.

In 2015, he joined the Radiation Laboratory, University of Michigan, as a Graduate Student Research Assistant. His current research interests include miniaturized antenna designs, electromagnetic scattering, and microwave photonics.

James F. Harvey (M'94–F'02) received the B.S. degree in engineering from the United States Military Academy, West Point, NY, USA, in 1964, the M.A. degree in physics from the Dartmouth College, Hanover, NH, USA, in 1972, and the Ph.D. degree in applied science from the University of California, Davis, CA, USA, in 1990.

He currently serves as an Research Program Manager for the Electronics Division Program on bioelectronics and nano-electronics with the U.S. Army Research Office, Durham, NC, USA. He also provides program assistance to the OSD Basic Research Office, Alexandria, VA, USA, for the Multidisciplinary University Research Initiative, Defense University Research Instrumentation Program, and the OSD Pilot Program: Innovation Corps at Department of Defense. His current research interests include electromagnetics, microwave circuit engineering, and optical materials.

Kamal Sarabandi (S'87–M'90–SM'92–F'00) received the B.S. degree in electrical engineering from the Sharif University of Technology, Tehran, Iran, in 1980, the M.S. degree in electrical engineering in 1986, and the M.S. degree in mathematics and the Ph.D. degree in electrical engineering from the University of Michigan, Ann Arbor, MI, USA, in 1989.

He possesses 25 years of experience with wave propagation in random media, communication channel modeling, microwave sensors, and radar systems, and leads a large research group including two research scientists and 16 Ph.D. students. He has graduated 46 Ph.D. and supervised numerous post-doctoral students. He has served as the Principal Investigator on many projects sponsored by the National Aeronautics and Space Administration (NASA), Jet Propulsion Laboratory, Army Research Office, Office of Naval Research, Army Research Laboratory (ARL), National Science Foundation, Defense Advanced Research Projects Agency, and a large number of industries. Currently, he is leading the Center for Microelectronics and Sensors funded in 2008 by the ARL under the Micro-Autonomous Systems and Technology Collaborative Technology Alliance Program. He is also leading a newly established center in Microwave Sensor Technology funded by King Abdulaziz City for Science and Technology. He is currently the Director of the Radiation Laboratory and the Rufus S. Teesdale Endowed Professor of engineering with the Department of Electrical Engineering and Computer Science, University of Michigan. He has authored many book chapters and over 250 papers in refereed journals on miniaturized and on-chip antennas, metamaterials, electromagnetic scattering, wireless channel modeling, random media modeling, microwave measurement techniques, radar calibration, inverse scattering problems, and microwave sensors, and over 580 papers and invited presentations in many national and international conferences and symposia on similar subjects. His current research interests include microwave and millimeter-wave radar remote sensing, metamaterials, electromagnetic wave propagation, and antenna miniaturization.

Dr. Sarabandi was selected as a fellow of the American Association for the Advancement of Science. He served as a member of the NASA Advisory Council appointed by the NASA Administrator for two consecutive terms from 2006 to 2010, and the Editorial Board of the PROCEEDINGS of the IEEE. He is a member of the Commissions F and B of URSI and is serving as the Vice Chair of the USNC URSI Commission F. He was a recipient of the Henry Russel Award from the Regent of the University of Michigan, the GAAC Distinguished Lecturer Award from the German Federal Ministry for Education, Science, and Technology in 1999, the 1996 EECS Department Teaching Excellence Award, the 2004 College of Engineering Research Excellence Award, the IEEE Geoscience and Remote Sensing Society (GRSS) Distinguished Achievement Award and the University of Michigan Faculty Recognition Award in 2005, the Best Paper Award at the 2006 Army Science Conference, the Humboldt Research Award from The Alexander von Humboldt Foundation of Germany in 2008, the Best Paper Award at the IEEE Geoscience and Remote Sensing Symposium, and the 2010 Distinguished Faculty Achievement Award from the University of Michigan. The IEEE Board of Directors announced him as the recipient of the 2011 IEEE Judith A. Resnik Award. He was recognized by the IEEE GRSS with its 2013 Education Award. He received the Stephen S. Attwood Award from the College of Engineering, University of Michigan, in 2016, and the Distinguished Alumni Award from the Sharif University of Technology. In the past several years, joint papers presented by his students at a number of international symposia (IEEE APS in 1995, 1997, 2000, 2001, 2003, 2005–2007, and 2016, IEEE IGARSS in 1999, 2002, 2007, 2011, and 2014, IEEE IMS in 2001, USNC URSI in 2004–2006, 2010, and 2011, AMTA in 2006, URSI GA in 2008 and 2014, and Eastern Snow Conference in 2016) have received best paper awards. He was an Associate Editor of the IEEE TRANSACTIONS ON ANTENNAS AND PROPAGATION and the IEEE SENSORS JOURNAL. Currently, he is serving as the President of the IEEE GRSS.